Journal of the Serbian Chemical Society
JSCS-info@shd.org.rs • www.shd.org.rs/JSCS
J. Serb. Chem. Soc. 80 (12) 1489–1504 (2015)
JSCS–4814
UDC 547.686+547.678.2:548.7:
543.424.2+543.42–74:519.677
Original scientific paper

X-Ray, Hirshfeld surface analysis, spectroscopic and DFT studies of polycyclic aromatic hydrocarbons: fluoranthene and acenaphthene

WIOLETA ŚMISZEK-LINDERT[1]*, ANNA MICHTA[2], ALEKSANDRA TYL[2], GRZEGORZ MAŁECKI[2], ELŻBIETA CHEŁMECKA[3] and SŁAWOMIR MAŚLANKA[2]

[1]Institute of Mechanized Construction and Rock Mining, W. Korfantego 193A Street, 40-157 Katowice, Poland, [2]Institute of Chemistry, University of Silesia, 9 Szkolna Street, 40-006 Katowice, Poland and [3]School of Pharmacy with Division of Laboratory Medicine in Sosnowiec, Medical University of Silesia, Katowice, Poland, Department of Statistics, 30 Ostrogórska Street, 41-200 Sosnowiec, Poland

(Received 4 March, revised 27 June, accepted 6 July 2015)

Abstract: The X-ray structure, theoretical calculation, Hirshfeld surfaces analysis, IR and Raman spectra of fluoranthene and acenaphthene were reported. Acenaphthene crystallizes in the orthorhombic crystal system and space group $P2_1ma$, with crystal parameters a = 7.2053(9) Å, b = 13.9800(15) Å, c = = 8.2638 (8) Å, Z = 4 and V = 832.41(16) Å^3. In turn, the grown crystals of fluoranthene are in the monoclinic system with space group $P2_1/n$. The unit cell parameters are a = 18.3490(2) Å, b = 6.2273(5) Å, c = 19.8610(2) Å, β = = 109.787(13)°, Z = 8 and the unit cell volume is 2135.50(4) Å^3. Theoretical calculations of isolated molecules of the title compounds were performed using DFT at the B3LYP level. The intermolecular interactions in the crystal structure, for both the title polycyclic aromatic hydrocarbons were analyzed using the Hirshfeld surfaces computational method.

Keywords: crystal structure; IR spectroscopy; Raman; density functional theory (DFT) calculation; Hirshfeld surfaces.

INTRODUCTION

Polycyclic aromatic hydrocarbons (PAHs) are important persistent organic pollutants (POPs) of the environment, which generally occur in all its parts: atmosphere, water, soils, sediments and vegetation.[1,2] The presence of PAHs in all these environmental elements may establish a risk for humans as well as all living organisms. Migration and distribution of PAHs in the environment depends on their physicochemical properties, *i.e.*, water solubility, octanol–water

* Corresponding author. E-mail: w.lindert@imbigs.pl
doi: 10.2298/JSC150304060S

distribution constant, or Henry's constants (volatility).[3–5] Besides, in the gas-phase of the atmosphere, PAHs can react with nitrogen oxides, ozone, OH radicals and NO_3 radicals, yielding, *e.g.*, nitrated, oxygenated, and hydroxylated derivatives of PAHs.[6–9] The nitrated PAH compounds are potentially more mutagenic and carcinogenic than the polycyclic aromatic hydrocarbon precursors.[10]

PAHs are released into the environment from domestic, industrial and natural sources. Anthropogenic PAHs are usually generated from incomplete combustion of fossil fuels (*e.g.*, oil, coal, crude oil, gasoline),[11,12] waste treatment,[11] combustion of synthetic chemicals,[11] and other human activities, such as cooking, tobacco smoking, or vehicle traffic.[13] The natural sources of emissions of PAHs pertain to forest fires,[11] volcanic eruptions[7] and carbonization processes, such as products of humus conversion by microorganisms,[14] diagenesis of organic matter,[15] *etc*.

Fluoranthene and acenaphthene are examples of PAHs, which are classified as priority control organic pollutants by the US Environmental Protection Agency (US EPA).[16] Acenaphthene is also on the Hazardous Substance List. Fluoranthene and acenaphthene are considered non-carcinogens for humans, but should be handled with caution.[17] Additionally, acenaphthene could be applied as an intermediary in pharmaceutical, agricultural and chemical industries.[17]

Molecular crystals of fluoranthene and acenaphthene, as well as their derivatives, were the subject of studies for the generation of the mechanism of their interactions by hydrogen bonds with other molecules in asphalt (a product from the distillation of petroleum). PAHs and their derivatives could be emitted from asphalt, and could migrate in the environment, for example, from contaminated soils into the ground water.[18] Therefore, they could be potential health hazards for humans.[19] The next aim of research is to obtain knowledge of the manner of interactions of PAHs and their derivatives with proteins by performing computer simulations using CLC Drug Discovery Workbench.[20] The experiments will be performed under conditions simulating the physiological pH.

EXPERIMENTAL

Materials

Fluoranthene (**I**) and acenaphthene (**II**) were provided by Sigma–Aldrich (Poland) at 98 and 99 % purity, respectively. The substances were investigated without further purification. Colourless crystals of **I,** suitable for X-ray analysis, were obtained by slow evaporation of ethanol–acetone mixture (1:1, *V*/*V*) at room temperature. On the other hand the crystals of acenaphthene were obtained upon recrystallization from petroleum ether, giving plate-shaped single crystals.

X-Ray crystal structure determination

The crystals of **I** and **II** were mounted in turn on a Gemini A Ultra Oxford Diffraction automatic diffractometer equipped with a CCD detector, and used for data collection. X-Ray intensity data were collected with graphite monochromated MoK_α radiation (λ = 0.71073 Å)

at room temperature, in the ω scan mode. Ewald sphere reflections were collected up to 2θ = = 50.10°. Lorentz, polarization and empirical absorption corrections using spherical harmonics implemented in SCALE3 ABSPACK scaling algorithm were applied.[21] The structures were solved by the direct method and subsequently completed by difference Fourier recycling. All non-hydrogen atoms were refined anisotropically using full-matrix, least-squares techniques. All hydrogen atoms were positioned in geometrically idealized positions and were allowed to ride on their parent atoms with U_{iso}(H) = 1.2 U_{eq}. The OLEX2[22] and SHELXS, SHELXL[23] programs were used for all calculations. Atomic scattering factors were those incorporated in the computer programs. All graphics were prepared using ORTEP-3[24] for Windows, Platon[25] and Mercury.[26]

Physical measurements

The infrared spectra of polycrystalline samples (dispersed in KBr pellets) and monocrystalline samples of fluoranthene and acenaphthene were recorded on a FT-IR Nicolet Magna 560 spectrometer in the transmission mode with 2 cm^{-1} resolution. The IR spectra of polycrystalline samples were measured at temperature 298 K, while the monocrystalline samples were measured at two temperatures, 298 and 77 K. The IR spectra were recorded in the spectral range of 4000–400 cm^{-1}. Crystals of **I** and **II** suitable for spectral studies were obtained by crystallization from melted samples occurring between two closely spaced CaF_2 windows. In this way, sufficiently thin crystals could be obtained, characterized by a maximum absorbance at the ν_{C-H} band frequency range close to 0.5. Monocrystalline fragments were selected from the crystalline mosaic and spatially oriented using a polarization microscope. In the next step, these selected crystals were exposed to the experiment with the use of a metal plate diaphragm with a 1.5 mm diameter hole. The Raman experiment was performed using a WITec confocal CRM alpha 300 Raman microscope (Jagiellonian Centre for Experimental Therapeutics – JCET, Kraków, Poland). The spectrometer was equipped with an air cooled solid state laser operating at 532 nm and CCD detector which was cooled to –58 °C. The laser was coupled to the microscope *via* a single mode optical fibre with a diameter of 50 μm. The scattered radiation was focused onto a multi-mode fibre (50 μm diameter) and a monochromator. A dry Olympus MPLAN (50×/0.76NA) objective was used. The integration time for a single spectrum was 2 s. The spectra were collected in the range between 4000–120 cm^{-1} with a spectral resolution of 3 cm^{-1}.

Theoretical calculations

The theoretical calculations were performed by means of the Gaussian 09[27] software package, using density functional theory (DFT) at the B3LYP level and with 6-31G(d,p) and 6-31G*(d,p) basis sets for acenaphthene, as well as 6-31+G(d,p) and 6-311++G(3df,2pd) basis sets for fluoranthene.[28,29]

The Hirshfeld surface analyses were realized using the CrystalExplorer program.[30] The distance from the Hirshfeld surface to the nearest nucleus inside and outside the surface were marked by d_i and d_e, respectively, whereas d_{norm} is a normalized contact distance, which is defined in turns of d_i, d_e and the van der Waals (vdW) radii of the atoms:[31]

$$d_{norm} = \frac{d_i - r_i^{vdW}}{r_i^{vdW}} + \frac{d_e - r_e^{vdW}}{r_e^{vdW}} \quad (1)$$

d_{norm} was visualized using a red–white–blue colour scheme. If the atoms make intermolecular contacts closer than the sum of their vdW radii, these contacts were represented as red spots

on the surface. Longer contacts were blue, while white was used for contacts around the sum of the van der Waals radii.[31]

RESULTS AND DISCUSSION

The crystal structures of fluoranthene (**I**) and acenaphthene (**II**) have already been described in the literature, *i.e.*, by Chakrabarti[32] and Hazell *et al.*,[33] and later by Munakata *et al.*[34], Ehrlich[35] and then by Hazell *et al.*,[36] respectively. The crystallographic data were re-collected in the present study because other conditions of crystals growth than in the literature were used, and these data were needed to perform the computer simulations of the binding processes of fluoranthene and acenaphthene with the selected human proteins.

The crystal data and final refinement details of compound **I** and **II** are given in Table I. The molecular structure of fluoranthene and acenaphthene are illustrated in Fig. 1a and b, respectively.

TABLE I. Crystal data and structure refinement details of fluoranthene (**I**) and acenaphthene (**II**)

Parameter	Fluoranthene (**I**)	Acenaphthene (**II**)
Empirical formula	$C_{16}H_{10}$	$C_{12}H_{10}$
Compound weight	202.24	154.20
Temperature, K	295.0(2)	295.0(2)
Crystal system	Monoclinic	Orthorhombic
Space group	$P2_1/n$	$P2_1ma$
Crystal dimension, mm	0.39 x 0.32 × 0.09	0.41 × 0.22 × 0.12
Crystal form, colour	Plate, colourless	Plate, colourless
	Unit cell dimensions	
a / Å	18.3490(2)	7.2053(9)
b / Å	6.2273(5)	13.9800(15)
c / Å	19.8610(2)	8.2638(8)
β / °	109.787(13)	90.00
V / Å^3	2135.50(4)	832.41(16)
Z	8	4
D_c / g cm^{-3}	1.258	1.230
F(000)	848	328
Θ range for data collection, °	4.0–29.2	4.8–27.5
Data collection method	ω scan	ω scan
Absorption coefficient, mm^{-1}	0.071	0.069
Final R indices ($I > 2\sigma(I)$)	R_1 =0.0696 , wR_2 = 0.1711	R_1 = 0.0442, wR_2 = 0.0964
R indices (all data)	R_1 = 0.1043, wR_2 = 0.1936	R_1 = 0.0550, wR_2 = 0.1022
Reflections collected/unique	2527 [R_{int} = 0.089]	1075 [R_{int} = 0.020]
Limiting indices	$-21 \le h \le 20$, $-7 \le k \le 7$, $-23 \le l \le 23$	$-8 \le h \le 6$, $-16 \le k \le 16$, $-7 \le l \le 9$
Refinement method	Full-matrix least-squares on F^2	Full-matrix least-squares on F^2
S	1.10	1.05
Parameters refined	289	105
$\Delta\rho_{max}$, $\Delta\rho_{min}$ / e Å^{-3}	0.22–0.21	0.25–0.28

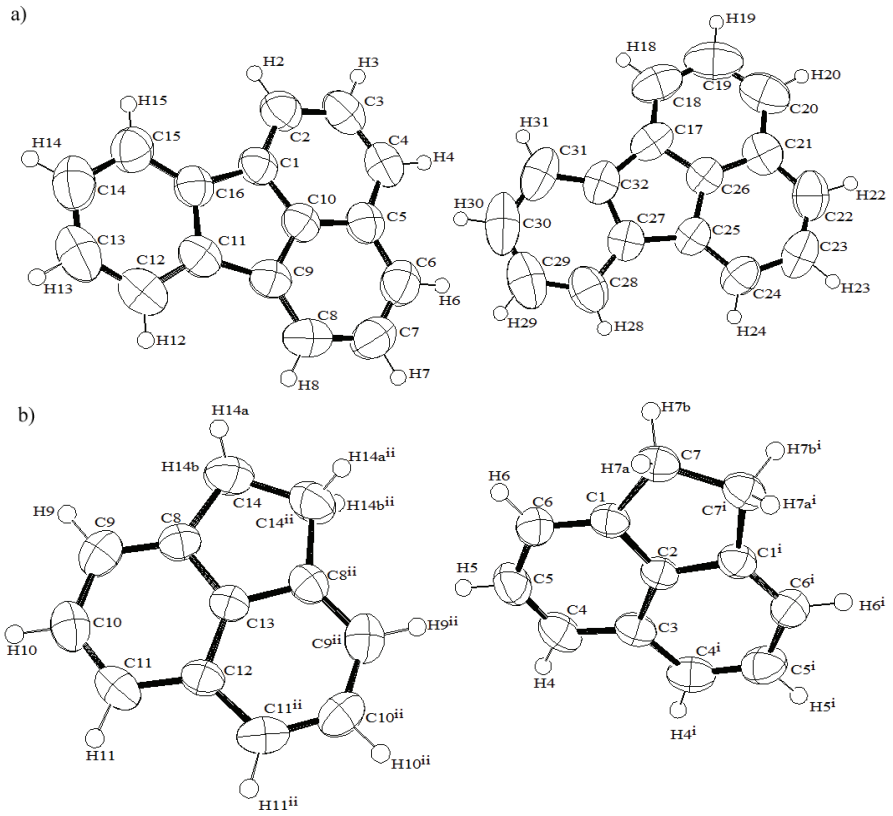

Fig. 1. The conformation of a) fluoranthene and b) acenaphthene molecules with the atom numbering scheme. Atomic displacement ellipsoids represent the 50 % probability level. H atoms are shown as small spheres of arbitrary radius. Symmetry code: *i*) *x*, *y*, *z*; *ii*) *x*, –*y*, *z*.

Compound **I** crystallizes with eight molecules in an asymmetric unit. The molecules in the unit cell are connected by weak C–H···π interactions between nearest neighbours. The intermolecular C–H···C interactions existing between carbon atoms of the condensed rings of the naphthalene structure nearest neighbouring molecules are shown in Fig. 2a (marked with blue dashed lines). Fluoranthene also contains π···π (C···C) interactions, but they are less dominant in this crystal structure. The C···C distances between neighbouring molecules are approximately 3.33 Å (Fig. 2a; red dashed line). Generally, the C···C van der Waals distance of 3.40 Å has been adopted as the reference distance for chemical stability.[37] Additionally, it is worth noting that the C···C distances are longer than the 2.6 Å distance observed in crystalline benzene.[38] The intermolecular C···C distance is also comparable to the C···C distance of dibenz[*a*,*h*]anthracene (3.37 Å).[39]

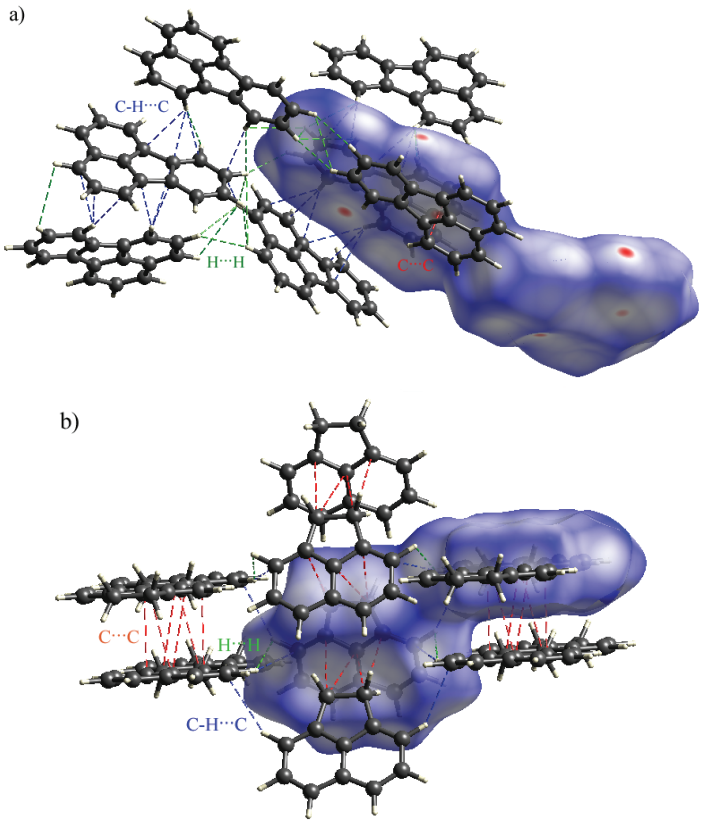

Fig. 2. Hirshfeld surfaces mapped with d_{norm} and part of the crystal structure of: a) fluoranthene and b) acenaphthene showing the intermolecular interactions.

The H···H contacts are marked green with a dashed line in Fig. 2a. The shortest close contacts between hydrogen atoms have a distance of approximately 2.37 Å (van der Waals radius for hydrogen atom is 1.2 Å). The shortest C–H···π close contacts have a distance of approximately 2.80 Å.

The intermolecular close contacts were likewise substantiated by examination of Hirshfeld surfaces. However, the fingerprint plots (2D representation of a Hirshfeld surface) provide a quantitative measure of the intermolecular interactions on the surface.[31,40] The C···H and H···C intermolecular interactions are depicted as two characteristic and distinct "spikes" in the two-dimensional fingerprint plot, Fig. 3a. The C···H (π···H) interactions (30.8 %) are represented by a spike (d_i = 1.74 Å, d_e = 1.75 Å) in the bottom right area of the fingerprint plot (these contacts are marked with a green ellipse; see Fig. 3a). Then the H···C (H···π) interactions (25.1 %) are represented by a spike (d_i = 1.74 Å, d_e = 1.75 Å) in the upper left area of the fingerprint plot (contacts are marked with a red

ellipse). Two small areas, visible on the fingerprint plot (Fig. 3b), are characteristic of π···π interactions (2.0 %). Besides, the presented results showed that the structure of **I** is also dominated by the H···H contacts (42.1 %), Fig. 3c.

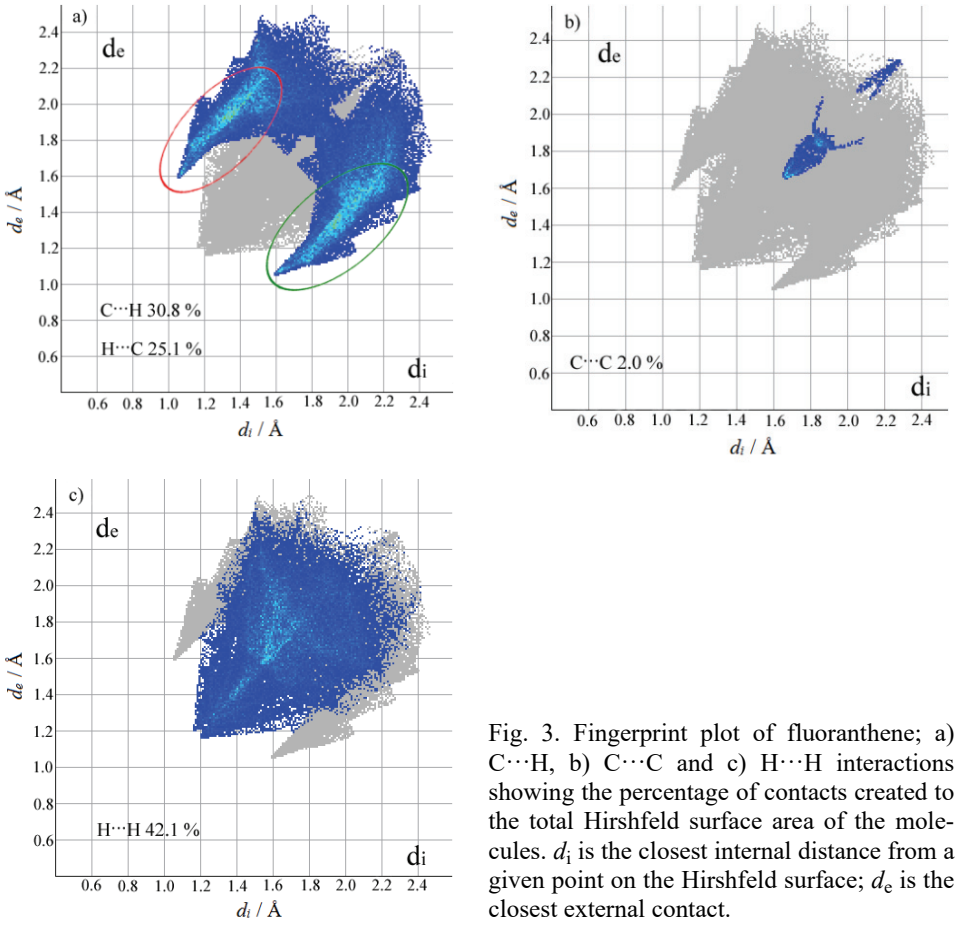

Fig. 3. Fingerprint plot of fluoranthene; a) C···H, b) C···C and c) H···H interactions showing the percentage of contacts created to the total Hirshfeld surface area of the molecules. d_i is the closest internal distance from a given point on the Hirshfeld surface; d_e is the closest external contact.

According to the classification of Desiraju and Gavezzotti,[41] the crystal packing of **I** follows a herringbone (HB) motif. The ratio of C···H to C···C interactions is 27.95 > 4.5.[42]

Hirshfeld surface analysis was also used for visual analysis of intermolecular interactions in the crystal structure of acenaphthene. The asymmetric unit of **II** contains four acenaphthene molecules that are linked by C–H···π interactions. The intermolecular C–H···C interactions, existing between carbon atoms of the condensed rings of the naphthalene structure nearest neighbouring molecules, are shown in Fig. 2b (blue dashed line). The shortest C–H···π close contacts have a distance of approximately 2.90 Å. The π···H (C–H) interactions provide 39.30

%, which is appreciably lower when compared to **I**. The C···H interactions (23.2 %) are represented by the characteristic wing (d_i = d_e = 1.66 Å) in the bottom right area of the fingerprint plot, Fig. 4a (contacts are denoted by a green ellipse). Then the H···C contacts (16.0 %) are illustrated by a wing (d_i = d_e = 1.66 Å) in the upper left area of the fingerprint plot, (the contacts are denoted by a red ellipse, see Fig. 4a).

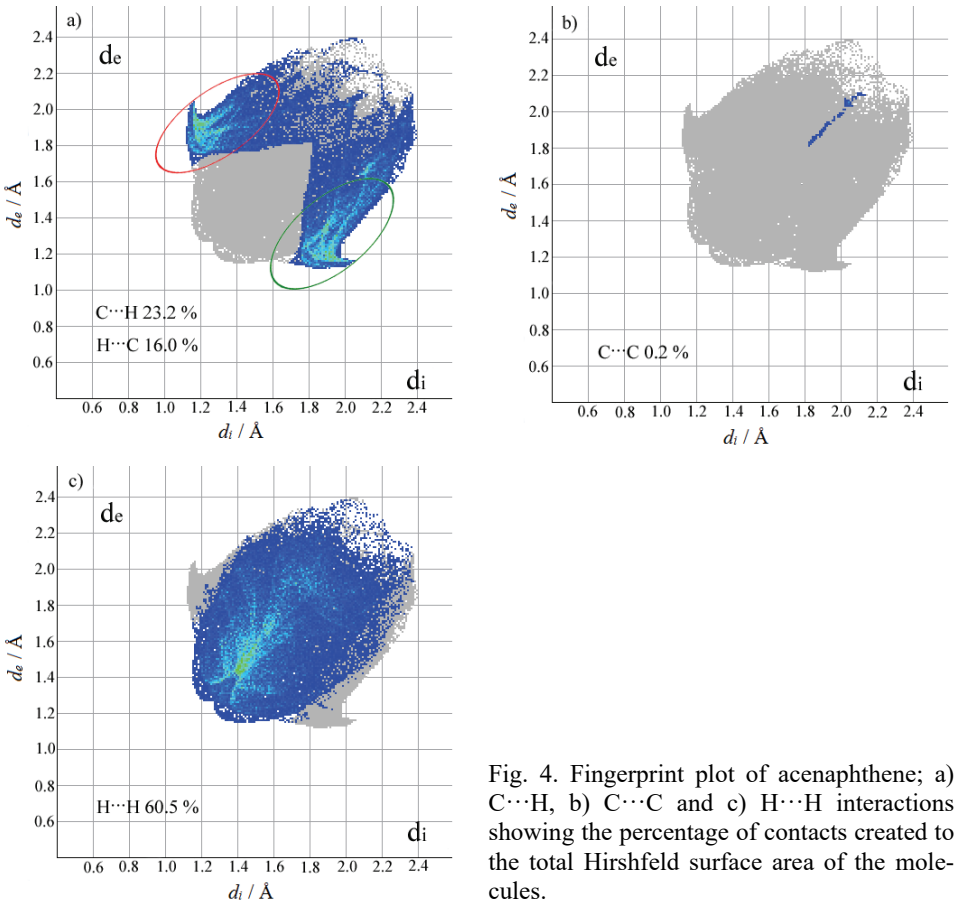

Fig. 4. Fingerprint plot of acenaphthene; a) C···H, b) C···C and c) H···H interactions showing the percentage of contacts created to the total Hirshfeld surface area of the molecules.

A significant difference between the molecular interactions in **I** and **II** in terms of H···H interactions is also noticeable in the fingerprint plots (Figs. 3c and 4c). In this case, H···H contacts comprise 60.5 % of the surface area. The shortest close contacts between hydrogen atoms have a distance of approximately 2.53 Å, Fig. 2b (green dashed line).

The π···π contacts are almost zero, and there are no significant interactions in the crystal structure of acenaphthene (C···C contacts make 0.2 % of the sur-

face area). The shortest close contacts between carbon atoms have a distance approximately 3.70 Å, Fig. 2b (red dashed line). The visual analysis of the fingerprint plots (C···H contact) of other PAHs, *e.g.*, naphthalene and anthracene, show that acenaphthene is more similar to them, than to fluoranthene.[43]

According to the method of Lootos and Barbour, the molecules of acenaphthene are arranged in a herringbone motif. The ratio of C···H to C···C is considerably greater than 4.5, and is 196.50.[42]

It should also be noted that in the unit cell, the molecules of fluoranthene and acenaphthene are not connected by hydrogen bonds. This fact was also proven by spectroscopic studies.

The Hirshfeld surface and 2D fingerprint plots were used for visualizing, exploring and quantifying intermolecular interactions in the crystal lattice of both PAHs. Besides, quantitative measures of Hirshfeld surfaces for fluoranthene and acenaphthene were obtained, such as molecular volume (V_H) 542,96 and 408,61 Å^3, surface area (S_H) 464,90 and 374,07 Å^2, globularity (G) 0.677 and 0.712, as well as asphericity (Ω) 0,456 and 0,333, respectively.

*IR spectra of compounds **I** and **II***

The IR spectra of polycrystalline samples of fluoranthene and acenaphthene, measured at 298 K using the KBr pellet technique, are shown in Fig. 5a and b, respectively. Additionally, the Raman spectra of **I** and **II** are also presented in Fig. 5a and b, respectively. The Raman spectra were measured at room temperature for polycrystalline samples. The Raman spectra allow for additional identification of the $\nu_{C–H}$ band positions, which are attributed to the C–H bond stretching vibrations in the molecules.[44]

Polarized IR spectra of **I** and **II** single crystals measured at 77 K, in the frequency ranges of the $\nu_{C–H}$ bands, are shown in Fig. 6a and b, respectively. The temperature dependence of the polarized crystalline spectra of fluoranthene and acenaphthene in the frequency ranges of the $\nu_{C–H}$ bands is presented in Fig. 7a and b, respectively.

The vibrations of crystalline acenaphthene can be divided into types: aromatic ring C–H stretching (3071–3036 cm^{-1}), CH_2 asymmetric stretching (2937––2914 cm^{-1}), CH_2 symmetric stretching (2840 cm^{-1}) (see Fig. 5b), in plane CH_2 group deformation (≈1423 cm^{-1}), aromatic ring stretching (≈1616–1593 cm^{-1}) and skeletal vibrations representing C=C stretching (≈1370 cm^{-1}). In Fig. 5b, C–H bending bands appear in the region 841–749 cm^{-1} (out-of-plane bending), and are very strong. In the case of crystalline fluoranthene, the characteristic IR bands in the five regions of the spectrum are illustrated in Figs. 5a and 6a. The main types of vibration are C–H stretching vibration, C=C stretching vibration, C–H out-of-plane vibration, C–H bending vibration and lattice vibration.[45]

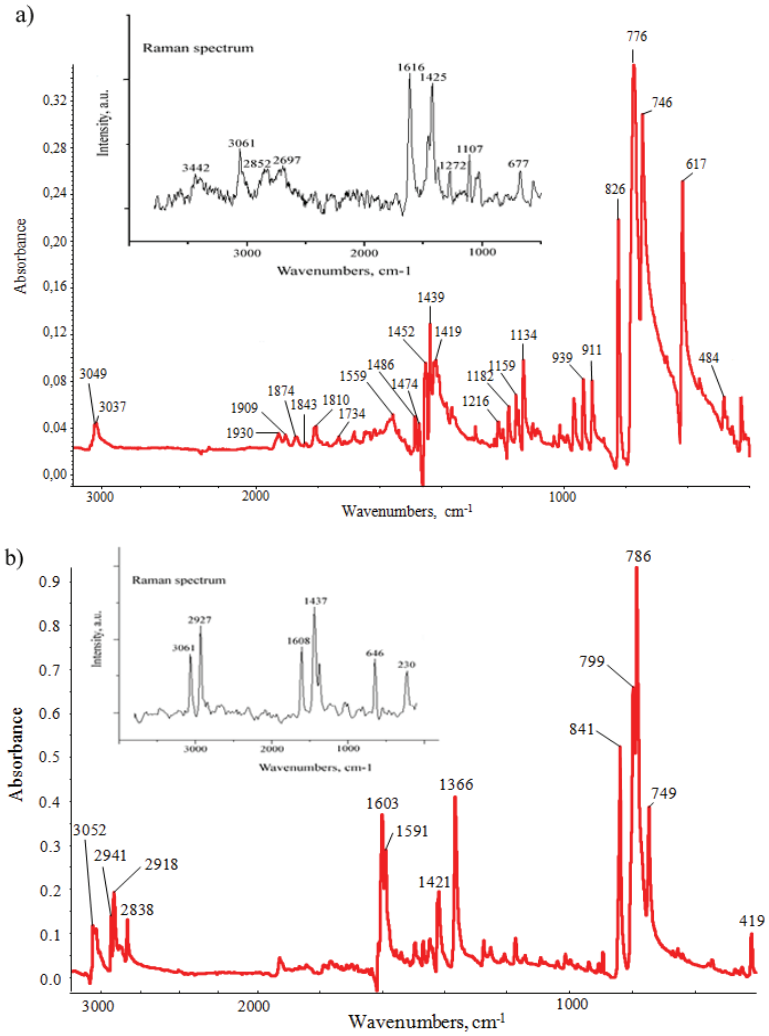

Fig. 5. IR spectra of polycrystalline samples of a) fluoranthene and b) acenaphthene measured at 298 K using the KBr pellet technique. Raman spectra for the identification of the vibration lines of the C–H bonds.

Analyzing the IR spectra of monocrystalline samples of acenaphthene, measured at the different orientations of the electric field vector *E*, the incident light on the crystal, large variability of the intensity of some bands could be observed, Fig. 6b. The ν_{C-H} bands (in the frequency range from 3060 to 2836 cm^{-1}) in the spectra of **II** crystals were characterized by the two-branch structure with their unique and relatively simple intensity distribution patterns. The polarized light

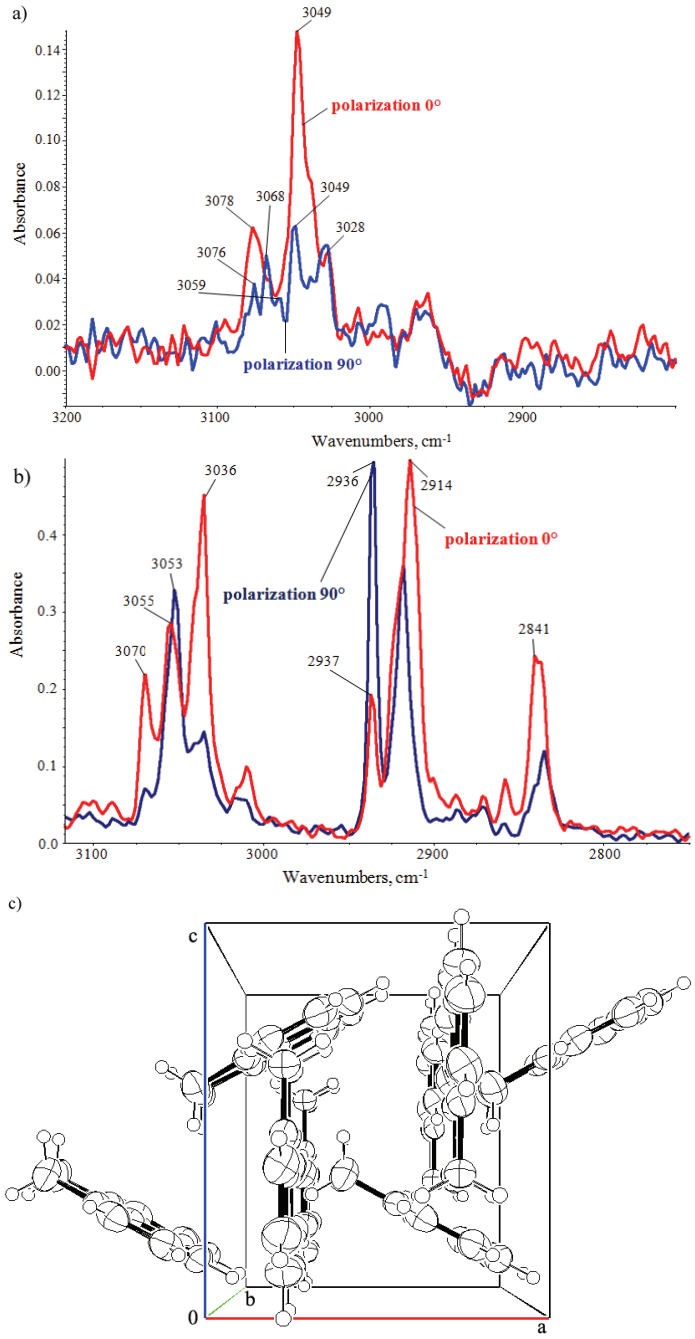

Fig. 6. Polarized spectra of a single crystal of: a) fluoranthene and b) acenaphthene measured at 77 K; c) packing diagram of acenaphthene viewed along the *b* axis.

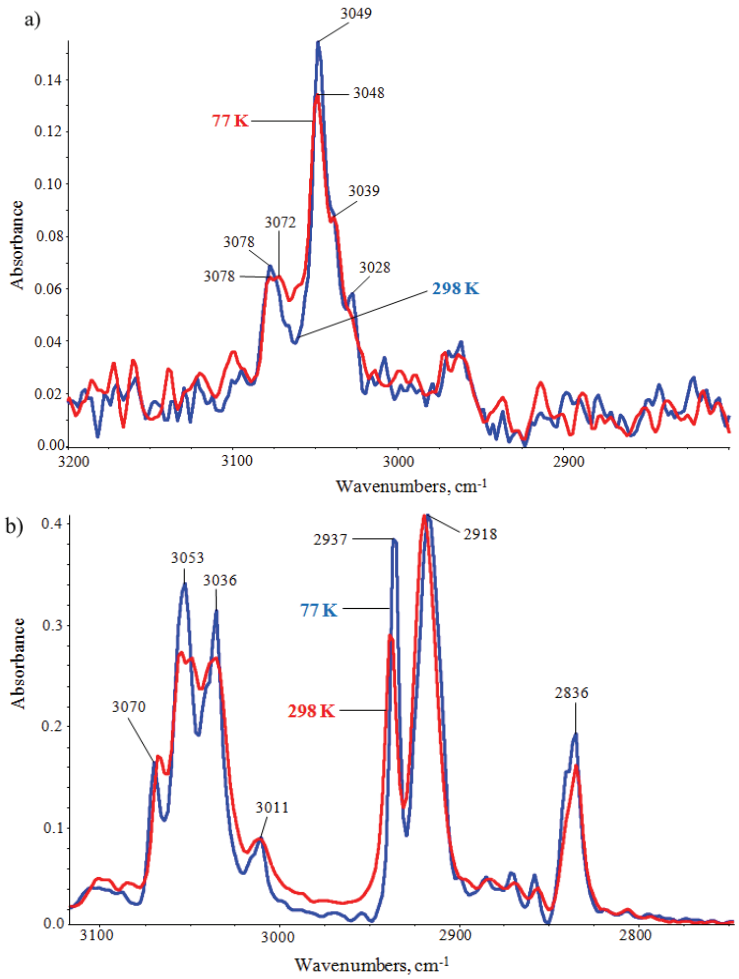

Fig. 7. Polarized spectra of a single crystal of: a) fluoranthene and b) acenaphthene are illustrative of the temperature effect.

especially strongly influenced the intensity of the bands of the stretching of C–H bonds vibrations in the molecules. Based on the results in Fig. 6b, it could be seen that the longer-wave branch (3060–3040 cm^{-1}) of the band was of relatively high intensity when compared with the branch properties of the shorter-wave band (3061–3075 cm^{-1}). These effects are related to the arrangement of the molecules in the unit cell. Two molecules lie in the crystalline plane *bc*, while the other two are arranged obliquely to them, Fig. 6c. Such an arrangement of the molecules means that, regardless of the type, C–H vibrations of different fragments of the molecules will be excited by the polarized light. Therefore, different intensity of the lines in the ν_{C-H} bands was observed in the spectra of the

acenaphthene crystals. For example, in the case of polarization 0°, the line 2937 cm^{-1} of the asymmetric CH_2 vibrations had significantly lower intensity compared with the 2914 cm^{-1} line (Fig. 6b). The opposite phenomenon was observed for polarization 90°. It may be noted that the polarization effects are also visible in some bands lying at lower frequencies.

The IR spectra of acenaphthene crystals showed that a temperature decrease to 77 K was responsible for a slight growth in the intensity of the longer-wave branch, whereas the intensity of the shorter-wave branch remained unchanged, Fig 7b.

Very similar phenomena were observed in the spectra of fluoranthene crystals (Figs. 6a and 7a). In this case, the largest differences in the intensities of the bands were also visible in the frequency range of the C–H bond stretching vibration in the molecules. On the other hand, the differences between the spectra measured at room temperature and the temperature of liquid nitrogen were a result of stiffening of the molecules. Therefore, there was a discernible sharpening of the $\nu_{C–H}$ bands contour, as well as a slight growth in their intensities.

The analysis of the IR and Raman spectra indicated that the skeletal vibrations of the C–C bands in the aromatic nucleus were much weaker in the IR spectra than in the Raman spectra. These data were also based on experimental data available in the literature.[44]

*DFT calculation results for compounds **I** and **II***

The studies showed satisfactory correlation between the calculated and XRD experimental structural parameters (Tables S-I and S-II of the Supplementary material to this paper). Significant differences in the DFT and XRD geometries were observed in case of fluoranthene in the C8–C9–C10–C1, C24–C25–C26––C17, C2–C1–C10–C9, C18–C17–C26–C25, C27–C25–C26–C21 and C32––C17–C26–C21 torsion angles, which had the values –178.5, –179.3, –179.5, –178.1, –178.7 and 179.1°, respectively.

Figure S-1 of the Supplementary material demonstrates a comparison of the calculated IR (non-scaled) spectra of fluoranthene and acenaphthene. It should be noted that the theoretical model satisfactorily reproduced the experimental infrared spectra for both PAHs. The results also showed slight discrepancies between the modelling and experimental data, which is not unusual since the calculations corresponded to the gas phase of a single isolated molecule, whereas the experiment was performed on crystal structures.

CONCLUSIONS

In the present paper, the crystal structure, the DFT calculations, analysis of Hirshfeld surfaces and fingerprint plots, as well as spectroscopic properties of the title PAHs are reported.

These results showed that Hirshfeld surface and fingerprint plot analysis provides rapid quantitative insight into intermolecular interactions in molecular solids. The close contacts, in the case of both analyzed compounds, are dominated by H···C (C–H···π) and H···H contacts and these relatively weak interactions have evident signatures in the fingerprint plots. In addition, it should be emphasized that the analysis of a Hirshfeld surface is well correlated to the spectroscopic studies. Moreover, the comparison of the DFT model with XRD in the present study may be considered good.

SUPPLEMENTARY MATERIAL

Calculated and XRD experimental structural parameters and calculated IR spectra of fluoranthene and acenaphthene are available electronically from http://www.shd.org.rs/JSCS/, or from the corresponding author on request.

CCDC-1011192 and CCDC-1011193 contain the supplementary crystallographic data for this paper. These data can be obtained free of charge at www.ccdc.cam.ac.uk/conts/retrieving.html or from the Cambridge Crystallographic Data Centre (CCDC), 12 Union Road, Cambridge CB2 1EZ, UK; fax: +44(0)1223-336033; e-mail: deposit@ccdc.cam.ac.uk

Acknowledgements. This work was founded by a grant of the Medical University of Silesia (No. KNW-1-026/N/5/0). All of the calculations were performed with the aid of hardware and software at the Wrocław Centre for Networking and Supercomputing WCSS, Wrocław, Poland.

ИЗВОД

РЕНДГЕНОСТРУКТУРНА АНАЛИЗА, МЕТОДА АНАЛИЗЕ ХИРШФЕЛДОВИХ ПОВРШИНА, СПЕКТРОСКОПСКА И DFT ИСПИТИВАЊА ФЛУОРАНТЕНА И АЦЕНАФТЕНА

WIOLETA ŚMISZEK-LINDERT[1], ANNA MICHTA[2], ALEKSANDRA TYL[2], GRZEGORZ MAŁECKI[2], ELŻBIETA CHEŁMECKA[3] и SŁAWOMIR MAŚLANKA[2]

[1]*Institute of Mechanized Construction & Rock Mining, W. Korfantego 193A Street, 40-157 Katowice, Poland,* [2]*Institute of Chemistry, University of Silesia, 9 Szkolna Street, 40-006 Katowice, Poland and* [3]*School of Pharmacy with Division of Laboratory Medicine in Sosnowiec, Medical University of Silesia, Katowice, Poland, Department of Statistics, 30 Ostrogórska Street, 41-200 Sosnowiec, Poland*

Дат је приказ рендгенске структуре, теоријских израчунавања, Хиршфелдове анализе површина, IR и Раманових спектара за флуорантен и аценафтен. Аценафтен кристалише као орторомбични кристални систем са $P2_1ma$ просторном групом и параметрима јединичне ћелије: a = 7,2053(9) Å, b = 13,9800(15) Å, c = 8,2638(8) Å, Z = 4 и V = = 832,41(16) Å^3. Супротно томе, флуорантен кристалише као моноклинични кристални систем са $P2_1/n$ просторном групом и следећим параметрима јединичне ћелије: a = = 18,3490(2) Å, b = 6,2273(5) Å, c = 19,8610(2) Å, β = 109,787(13)°, Z = 8 и V = 2135,50(4) Å^3. Теоријска израчунавања за изоловане молекуле наведених једињења су извршена помоћу DFT израчунавања и B3LYP методе. Применом Хиршфелдове компјутерске методе засноване на анализи површина одређене су интермолекулске интеракције у кристалним структурама оба PAHs једињења.

(Примљено 4. марта, ревидирано 27. јуна, прихваћено 6. јула 2015)

REFERENCES

1. A. Mrozik, Z. Piotrowska-Seget, S. Łabużek, *Pol. J. Environ. Stud.* **12** (2003) 15
2. B. Maliszewska-Kordybach, *Pol. J. Environ. Stud.* **8** (1999) 131
3. A. Baklanov, O. Hänninen, L. H. Slørdal, J. Kukkonen, N. Bjergene, B. Fay, S. Finardi, S. C. Hoe, M. Jantunen, A. Karppinen, A. Rasmussen, A. Skouloudis, R. S. Sokhi, J. H. Sørensen, V. Ødegaard, *Atmos. Chem. Phys.* **7** (2007) 855
4. K. H. Kim, S. A. Jahan, E. Kabir, R. J. C. Brown, *Environ. Int*. **60** (2013) 71
5. M. J. Ahrens, C. V. Depree, *Chemosphere* **81** (2010) 1526
6. A. J. Cohen, *Environ. Health Persp*. **108** (2000) 743
7. M. P. Holloway, M. C. Biaglow, E. C. McCoy, M. Anders, H. S. Rosenkranz, P. C. Howard, *Mutat. Res*. **187** (1987) 199
8. D. Helmig, J. Arey, R. Atkinson, W. P. Harger, P. A. McElroy, *Atmos. Environ., A* **26** (1992) 1735
9. J. Arey, B. Zielinska, R. Atkinson, A. M. Winer, T. Ramdahl, I. N. Pitts, *Atmos. Environ.* **20** (1986) 2339
10. Y. Zhang, S. Tao, *Atmos. Environ.* **43** (2009) 812
11. J. Lewtas, *Mutat. Res.* **636** (2007) 95
12. K. Ravindra, R. Sokhi, R. Van Grieken, *Atmos. Environ.* **42** (2008) 2895
13. M. A. Bari, G. Baumbach, B. Kuch, G. Scheffknecht, *Air Qual. Atmos. Health* **3** (2010) 103
14. K. Skupińska, I. Misiewicz, T. Kasprzycka-Guttman, *Acta Pol. Pharm*. **61** (2004) 233
15. K. Banger, G. S. Toor, T. Chirenje, L. Ma, *Soil Sediment Contam*. **19** (2010) 231
16. EPA United States Environmental Protection Agency, *Priority Pollutants*, http:// //water.epa.gov/scitech/methods/cwa/pollutants.cfm (accessed 21 February 2015)
17. Agency for Toxic Substances and Disease Registry (ATSDR), *Toxicological profile for aromatic hydrocarbons*, U.S. Department of Health and Human Services, U.S. Public Health Services, Washington D.C., 1990, pp. 7, 226
18. I. R. DeLeon, C. J. Byrne, E. L. Peuler, S. R. Antoine, J. Schaefer, R. C. Murphy, *Chemosphere* **15** (1986) 795
19. S. Binet, P. Bonnet, H. Brandt, M. Castegnaro, P. Delsaut, J. F. Fabries, C. K. Huynh, M. Lafontaine, G. Morel, H. Nunge, B. Rihn, T. Vu Duc, R. Wrobel, *Ann. Occup. Hyg*. **46** (2002) 617
20. CLC Drug Discovery Workbench 2.4, 2015 CLC bio, QIAGEN Company
21. Oxford Diffraction, CrysAlis CCD & CrysAlis RED, Version 1.171.29.2, Oxford Diffraction Ltd., Wrocław, Poland, 2006
22. O. V. Dolomanov, L. J. Bourhis, R. J. Gildea, J. A. K. Howard, H. Puschmann, *J. Appl. Crystallogr*. **42** (2009) 339
23. G. M. Sheldrick, *Acta Crystallogr., A* **64** (2008) 112
24. L. J. Farrugia, *J. Appl. Cryst*. **45** (2012) 849
25. A. L. Spek, *Acta Crystallogr., D* **65** (2009) 148
26. C. F. Macrae, P. R. Edgington, P. McCabe, E. Pidcock, G. P. Shields, R. Taylor, M. Towler, J. van de Streek, *J. Appl. Crystallogr.* **39** (2006) 453
27. Gaussian 09, Revision A.02, Gaussian, Inc., Wallingford, CT, 2009
28. A. D. Becke, *J. Chem. Phys*. **98** (1993) 5648
29. C. Lee, W. Yang, R. G. Parr, *Phys. Rev., B* **37** (1998) 785
30. S. K. Wolff, D. J. Grimwood, J. J. McKinnon, D. Jayatilaka, M. A. Spackamn, *Crystal Explorer 3.0*, University of Western Australia, Perth, 2007
31. M. A. Spackman, D. Jayatilaka, *CrysEngComm* **11** (2009) 19

32. S. C. Chakrabarti, *Proc. Natl. Inst. Sci. India* **21** (1955) 263
33. A. C. Hazell, D. W. Jones, J. M. Sowden, *Acta Cryst*. **33** (1977) 1516
34. M. Munakata, L. P. Wu, G. L. Ning, T. Kuroda-Sowa, M. Maekawa, Y. Suenaga, N. Maeno, *J. Am. Chem. Soc*. **121** (1999) 4968
35. H. W. W. Ehrlich, *Acta Crystallogr*. **10** (1957) 699
36. A. C. Hazell, R. G. Hazell, L. Nørskov-Lauritsen, *Acta Crystallogr*. **42** (1986) 690
37. B. Schatschneider, J. J. Liang, *J. Chem. Phys*. **135** (2011) 164508
38. L. Ciabini, M. Santoro, F. A. Gorelli, R. Bini, V. Schettino, S. Raugei, *Nature Mater*. **6** (2007) 39
39. J. M. Robertson, J. G. White, *J. Chem. Soc*. (1956) 925
40. P. A. Wood, J. J. McKinnon, S. Parsons, E. Pidcock, M. A. Spackman, *CrystEngComm* **10** (2008) 368
41. G. R. Desiraju, A. Gavezzotti, *Acta Crystallogr., B* **45** (1989) 473
42. L. Loots, L. J. Barbour, *CrystEngComm* **14** (2012) 300
43. A. Parkin, G. Barr, W. Dong, C. J. Gilmore, D. Jayatilaka, J. J. McKinnon, M. A. Spackman, C. C. Wilson, *CrystEngComm* **9** (2007) 648
44. H. T. Flakus, W. Śmiszek-Lindert, K. Stadnicka, *Chem. Phys*. **335** (2007) 221
45. M. Hesse, H. Meier, B. Zeeh, *Spectroscopic Methods in Organic Chemistry*, Thieme, Stuttgart, 2007, p. 72.